Multispectral remote sensing algorithms for particulate organic carbon (POC): the Gulf of Mexico

Young Baek Son[a,b], Wilford D. Gardner[b], Alexey V. Mishonov[c], and Mary Jo Richardson[b]

[a] Department of Fisheries
Nagasaki University
1-14 Bunkyo, Nagasaki
Nagasaki, Japan 852-8521

[b] Department of Oceanography
Texas A&M University
College Station
Texas, USA, 77843-3146

[c] National Oceanographic Data Center
1315 East West Highway
Silver Spring, MD, 20910-3282

Corresponding Author:
Young Baek Son
Tel.: 81-95-819-2804
E-Mail: sonyb@nagasaki-u.ac.jp

Abstract

To greatly increase the spatial and temporal resolution for studying carbon dynamics in the marine environment, we have developed remote sensing algorithms for particulate organic carbon (POC) by matching in-situ POC measurements in the Gulf of Mexico with matching SeaWiFS remote sensing reflectance. Data on total particulate matter (PM) as well as POC collected during nine cruises in spring, summer and early winter from 1997-2000 as part of the Northeastern Gulf of Mexico (NEGOM) study were used to test algorithms across a range of environments from low %POC coastal waters to high %POC open ocean waters. Finding that the remote-sensing reflectance clearly exhibited a peak shift from blue to green wavelengths with increasing POC concentration, we developed a maximum normalized difference carbon index (MNDCI) algorithm which uses the maximum band ratio of all available blue-to-green wavelengths, and provides a very robust estimate over a wide range of POC and PM concentrations (R^2=0.99, N=58). The algorithm can be extrapolated throughout the region of shipboard sampling for more detailed coverage and analysis.

Keywords: Particulate Organic Carbon (POC), Satellite ocean color algorithm, Maximum normalized difference carbon index (MNDCI), SeaWiFS, the Gulf of Mexico

1. Introduction

As we strive to better understand carbon cycling in the ocean, it is important to be able to measure particulate organic carbon (POC) as well as dissolved organic and inorganic constituents effectively. POC generally may be a small component of the total carbon, but since POC can sink through the water column, it plays an important role in sequestering carbon and transporting associated elements and compounds downward as part of the biological pump.

The Gulf of Mexico, a semi-enclosed ocean, is biologically productive in the shelf environments and has a physically complex circulation system (Ohlmann & Niiler, 2005; Vastano et al., 1995; Walker, 1996). Several rivers along the surrounding land discharge a large mass of fresh water to the shelf along with high concentrations of dissolved and particulate organic and inorganic matter and pollutants (Morey et al., 2003; Walker et al., 1994). The largest riverine source is the Mississippi-Atchafalaya System (Walker et al., 1994), which drains approximately 40% of the continental United States. Due to the input of organic and inorganic materials, the Mississippi River plume has been identified as a potentially important factor in the high level of primary production found in the northern Gulf of Mexico, and strongly influences seasonal and inter-annual circulation patterns of that region (Lohrenz et al., 1990; Rabalais et al., 1996; Redalje et al., 1994; Walker, 1996).

Spatial and temporal variations in particle concentrations in the Gulf of Mexico are influenced by the seasonal and inter-annual variations of the local shelf and mesoscale circulations. These conditions can sometimes cause negative impacts

resulting from high productivity, elevated organic matter concentrations, and export from the euphotic zone causing "dead zones" of hypoxia along the Gulf Coast west of the Mississippi (Rabalais et al., 1996). The North-East Gulf of Mexico (NEGOM), Louisiana-Texas Shelf Physical Oceanography Program (LATEX), and hypoxia studies around the Mississippi River outflow have provided useful information for characterizing the oceanic environment of the northern Gulf of Mexico region (Cho et al., 1998; DiMarco & Reid, 1998). These studies have greatly expanded our knowledge on many parameters of the carbon pool as well as hydrography. However, measurements of POC have been made primarily in a limited number of programs. In order to expand coverage, *in situ* optical and remote sensing approaches are desperately needed to assess the distribution of POC in a variety of oceanic environments on different spatial and temporal scales.

Over the past three decades, most efforts have focused on predicting the concentration of marine chlorophyll *a* using empirical relationships between spectral reflectance or, equivalently, normalized water leaving radiance and chlorophyll *a* pigment concentration (Afonin et al., 1992; O'Reilly et al., 1998, 2000; Sathyendranath et al., 1989). Several algorithms have been developed based on optical closure relationships using model-based approaches to reveal links between reflectance spectra or normalized water leaving radiance and relevant inherent optical properties (IOP) of seawater, namely, the backscattering and absorption coefficients (Carder et al., 1999; Garver & Siegel, 1997; Maritorena et al., 2002; Roesler & Perry, 1995). The goal of such efforts is to obtain reasonable coverage to monitor spatial and temporal changes in

chlorophyll and derived products such as primary production (Behrenfeld et al., 2005) for a variety of environmental and ecological studies.

While chlorophyll is a component of POC, it is only a small percentage (<~2%; Chung et al., 1998), and not all POC contains chlorophyll. To better understand the cycling of POC in surface waters, algorithms have been developed for the open ocean (Gardner et al., 2006; Loisel et al., 2001; Mishonov et al., 2003; Stramska & Stramski, 2005; Stramski et al., 1999; 2008).

In the first published algorithm for estimating POC from remote sensing, Stramski et al. (1999) used a two-step process to calculate POC concentrations. First they correlated POC concentration with the *in-situ* particulate backscattering coefficient, b_{bp}. The second relationship linked remote-sensing reflectance R_{rs} with $b_{bp.}$ Measurements were made in the green spectral band. They used the remote-sensing reflectance at 555 nm ($R_{rs}(555)$) for correlation/normalization instead of $L_{wn}(555)$. Stramski et al. (2008) further refined this approach using data from two regions of the Pacific Ocean and Atlantic Ocean and found the best power function fits to be for POC vs $R_{rs}(443)/R_{rs}(555)$, and vs $R_{rs}(490)/R_{rs}(555)$. A single-wavelength approach using $L_{wn}(555)$ correlated with beam attenuation due to particles (c_p) was later developed and used to estimate surface POC concentration in the South Atlantic by means of a c_p/POC regression (Mishonov et al., 2003) and a similar approach using K_{490} was tested in the Pacific Southern Ocean and the Gulf of Mexico (Gardner et al., 2006).

While these algorithms provide a reasonable assessment of POC distribution in the open ocean on regional to global scales, further assessment is needed to be sure that

algorithms can predict POC concentrations in coastal waters. As with chlorophyll, the ability to remotely determine POC concentrations is important for quantifying the time-varying evolution of POC in surface waters to monitor, and eventually model, the impact of climate change on surface water productivity and loss.

The purpose of this paper is to develop accurate and efficient POC algorithms in the Gulf of Mexico based on satellite products by comparing POC estimates with *in situ* measurements, and to demonstrate how the improved resolution in mapping POC distributions improve our ability to understand, monitor, and eventually to model temporal and spatial variability of POC in complex oceanic environments.

2. Methods and Data

2.1. In situ Shipboard Data

During the Northeastern Gulf of Mexico project (NEGOM), data from approximately 100 CTD/transmissometer/fluorometer casts were collected on each of nine cruises from November 1997 to August 2000 along the same eleven track lines. Each seasonal cruise was completed along lines normal to the coastline between mid-Florida and the Mississippi River, starting from about 20 m water depth on the shelf and moving out to the 1000 m isobath (Fig. 1). This area spans a wide range of particle concentrations and types, from turbid river runoff to clear, open-ocean waters. Hydrographic data (temperature, salinity), including beam attenuation due to particles (c_p, λ=660 nm), were collected at each station. Water samples from the CTD rosette were filtered to obtain concentrations of particulate organic carbon (POC) and particulate matter (PM) at about ~60 of the stations. Samples were collected from the surface (1-10m) and near bottom with occasional additional samples within the first attenuation depth of light or at attenuation/fluorescence maxima.

For PM sampling, 47-mm diameter, 0.4-μm pore size polycarbonate membrane filters were triple-weighed prior to each cruise. After filtering 1-3 liters the filters were dried at approximately 30°C for 3-4 hours and triple-weighed after the cruise. For each cruise, several blanks were subjected to the same weighing process, taken to sea, and reweighed after the cruise to serve as blank corrections. No water was passed through these filters (Bernal, 2001; Gardner et al., 1993).

For POC sampling, 1-3 liters of water were filtered through 25-mm diameter GF-75 glass-fiber filters (approximately 0.7-µm pore size) that had been pre-combusted in a Thermolyne Type 1300 furnace along with aluminum foil squares. The filters were then wrapped in aluminum foil and dried at approximately 30°C for 3-4 hours. Prior to analysis, filters were acidified to remove carbonates, and then combusted converting the organic carbon to CO_2, which was then measured by thermal conductivity. Blanks were subtracted as described in protocols for JGOFS (JGOFS, 1996). When multiple surface samples were obtained at a station, their POC values were averaged for this analysis.

A SeaTech 25-cm pathlength (r) transmissometer was used to measure beam attenuation coefficient due to particles (c_p), at a wavelength of 660 nm (± 10 nm) using standard protocols (Gardner et al. 2006). Values of c_p were then plotted against the corresponding discrete POC and PM concentrations to determine the correlation between POC/PM and c_p, thus providing predictive capability of the POC and PM concentration based on the optical beam attenuation. A few outlying points were examined and removed if they were collected at depths of large vertical gradients in c_p.

2.2. Satellite Data

Daily SeaWiFS satellite images (1-km Level 1A) covering the Gulf of Mexico were obtained from NASA (http://oceancolor.gsfc.nasa.gov/). The spectral normalized water-leaving radiance (L_{wn}) was derived from the SeaWiFS Level 2 data with SeaDAS MSL12 processing code (Baith et al., 2001; McClain et al., 2004) using the standard Gordon and Wang (1994) atmospheric correction to derive L_{wn} and remotely-sensed

reflectance (R_{rs}) at 412, 443, 490, 510, 555, and 670 nm. R_{rs} was calculated as $R_{rs}(\lambda)= L_{wn}(\lambda)/F_0$, where F_0 is the mean extraterrestrial solar irradiance at a given spectral band. The derived spectral data were used to estimate POC and calculate the chlorophyll concentration and diffuse attenuation coefficient at 490 nm (K_{490}) using the standard SeaWiFS algorithms (Mueller, 2000; O'Reilly et al., 2000).

2.3. Empirical Approach

To estimate POC concentration using an empirical match-up approach, we matched concentrations of ship-collected POC samples with synchronously obtained satellite-derived ocean color data. We recognize that it may be desirable to have in-water optical measurements in the development of satellite algorithms, but that was not an objective of the original NEGOM program, so this study is a post-cruise analysis of the *in situ* POC data matched with satellite data that are available.

The matching of spectral data was initially restricted to a narrow area when the satellite passed our *in situ* sampling location at local noon. However, it was temporally and spatially impossible to match up a significant portion of the data set in this manner. In order to expand our temporal and spatial data coverage for comparing SeaWiFS and hydrographic data, we adopted the NASA Ocean Biology Processing Group's (OBPG) approach (Bailey et al., 2000; Bailey & Werdell, 2006). In the temporal window the SeaWiFS data were extracted for the location of NEGOM stations when *in-situ* and satellite measurements were made within a ±3 hour window (Bailey & Werdell, 2006) of local noon (0900 – 1500 local time). In order to obtain a reasonable balance between the

geophysical homogeneity of the sampling matrix and number of clear pixels in the spatial window, Bailey and Werdell (2006) argued that satellite data must meet the following conditions: 1) the size of the matrix of satellite data used does not significantly degrade the geophysical homogeneity among pixels used, and 2) >50% of the pixels are free of clouds or other errors. In our study we found that a 3×3 pixel grid met the above conditions; that is, this matrix size provided enough pixels to provide confidence in the average value, but not so large as to cross parameter gradients. Although uncertainties exist between *in situ* measurements and satellite-derived ocean color products based on pixel-by-pixel or averaging of pixels found, such match-up approaches (McClain et al., 2000) are essential for using satellite data. 58 POC sub-samples, about 11 % of the total 526 POC samples, were matched with the SeaWiFS spectral data using the above and following criteria:

1) the effect of outliers on the calculation was reduced by applying the filtered mean method (Bailey & Werdell, 2006) as $\frac{\sum_i (\overline{X} - 1.5 \times \sigma) < X_i < (\overline{X} + 1.5 \times \sigma)}{N}$.

where $\overline{X}$ is the unfiltered mean value, σ is the standard deviation of the unfiltered data and N is the number of values within $\pm 1.5 \times \sigma$.

2) the *in-situ* POC values were compared with the revised mean values of SeaWiFS-derived chlorophyll *a*, K_{490}, normalized water leaving radiance L_{wn}, and remotely-sensed reflectance R_{rs} for all spectral bands; and

3) least-squares fit methods were used for multiple and linear regressions.

3. Results and Discussions

3.1. Water Mass Classification Using Beam Attenuation, POC, and PM

Previous efforts at correlating POC with ocean color have focused on open-ocean data (Gardner et al., 2006; Loisel et al., 2001; Mishonov et al., 2003; Stramska & Stramski, 2005; Stramski et al., 1999; 2008). Our NEGOM data come from both open-ocean and coastal waters influenced by river input, which were originally classified as Case 1 and Case 2 waters (Morel & Prieur, 1977). Recent analyses of this classification have better articulated the definitions of water types and their complexity as more remote optical measurements become available and our understanding of optics and ecology increase. Mobley et al. (2004) and Lee and Hu (2006) suggest the abandonment of the Case 1 – Case 2 classification.

In an attempt to optically differentiate water types, we sought to take advantage of having both POC and PM data from the same samples by classifying waters based on the percentage of POC relative to PM (%POC=(POC/PM) x 100). We first tested this differentiation in the relationship between POC and beam attenuation coefficient due to particles at 660 nm (c_p) as illustrated in Fig. 2a. A linear regression between POC and c_p revealed a reasonable relationship (R^2=0.64, N=500), but scatter increased at higher POC concentrations (Fig. 2a). Other studies have shown much tighter correlations between beam attenuation and POC concentration (Bishop, 1999; Bishop et al., 1999; Chung et al., 1998; Gardner et al., 1993, 1995, 2003, 2006; Loisel & Morel, 1998; Mishonov et al., 2003; Stramska & Stramski, 2005; Stramski et al., 1999), but previous

studies primarily used data from open ocean environments, that did not include coastal areas close to the output of large rivers.

The c_p data are not used in our remote sensing algorithms, but the marked improvement in the c_p-POC correlation suggested this would be a useful differentiation in developing remote sensing algorithms. All 500 data points (Fig. 2a) were separated at the >25%, <25% point to distinguish between samples dominated by organic and inorganic components (Fig. 2c and 2d). The 25% dividing point is empirical, determined by the highest R value tested at 2.5 % increments. Fig. 2c shows that POC concentrations from samples with POC >25% were significantly better correlated with c_p (R^2=0.87, N=244).

$$POC = 326.6 \times c_p + 2.0 \quad (1)$$

The slope of our regression is similar to the results of studies in other oceans using bottle-collected POC (Fig. 2b). These results confirm that c_p provides a good estimate of POC when samples are primarily biogenic particles, and we expected that the compositional difference might have an impact on satellite POC algorithms as well.

Samples where POC <25% contain relatively more terrigenous particles and potentially CDOM, which can cause significant differences due to variations in their absorption/scattering properties compared with phytoplankton. In the Gulf of Mexico study area these zones are not always delineated geographically or by water depth, because river plumes, the loop-current, and eddies are always moving, so high %POC (>25%) and low %POC (<25%) was a useful first-order differentiation between water types.

3.2. Empirical Approach with POC and SeaWiFS Products (Chlorophyll or K_{490})

In this study we test several approaches in order to find the most reliable algorithms for estimating POC directly from remote-sensing products. In the first approach we use an empirical property-property match-up and calculate a regression between POC and chlorophyll concentrations using a logarithmic-fit that results in equation 2, which yields a well-correlated relationship (R^2=0.97, N=58, Fig. 3a): .

$$POC = 10^{(0.71 \times \log_{10}(chl)+2.2)} \quad (2)$$

where *chl* is derived from the standard SeaWiFS-OC4v4 chlorophyll algorithm, which is based on a ratio of blue/green reflectance (O'Reilly et al., 2000). Note that in this correlation we use only the 58 points where *in-situ* POC and SeaWiFS chlorophyll *a* are collected synchronously as defined earlier. In the POC-Chlorophyll *a* relationship there is only a slight difference between samples where POC is less than or greater than 25% (Fig. 3a, 7a and Table 1).

Our regression in Fig. 3a is in fair agreement with the relationships determined by Loisel and Morel (1998), Mishonov et al. (2003) and Stramska and Stramski (2005), all based on open-ocean data. POC algorithms of Mishonov et al. (2003) used data averaged over 5 years from the South Atlantic Ocean, Stramska and Stramski (2005) used data from the North Atlantic Ocean, and Loisel and Morel (1998) used data from the North Atlantic and Pacific Ocean, so deviations are likely due to regional differences.

Behrenfeld et al. (2005) argue that in general, POC concentration is well correlated with phytoplankton carbon, which is strongly suggested by the tight

correlation in Fig. 3a, although earlier studies state that phytoplankton carbon represents only 19-49% of POC (DuRand et al., 2001; Eppley et al., 1992; Gundersen et al., 2001). Cho and Azam (1990) suggested that the sum of bacterial carbon and phytoplankton carbon generally adds-up to about one-half of total POC.

Using the same approach as with chlorophyll a, we made an empirical match-up between NEGOM POC and $K_{490,}$ the downwelling diffuse attenuation at 490nm, and calculated a regression using a logarithmic fit that results in equation 3.

$$POC = 10^{(1.2\times\log_{10}(K_{490})+3.3)} \quad (3)$$

where K_{490} is derived from an algorithm using the standard SeaWiFS diffuse attenuation coefficient at 490 nm (Mueller, 2000).

As with the chlorophyll-POC correlation, POC concentrations based on K_{490} data are also slightly different between samples where POC is less than or greater than 25% (R^2=0.95, N=58, Fig. 3b, 7b and Table 1). The standard SeaWiFS K_{490} algorithm uses the ratio of $L_{wn}(490)$ to $L_{wn}(555)$, but the wavelength of the peak radiance varied between 490 nm and 555 nm, particularly over green and brown coastal water (Dudek et al., 2003). An algorithm by Mishonov et al. (2003) for other oceans closely predicts the relationship between POC and chlorophyll in the Gulf of Mexico (Fig. 3a). The algorithms of both Mishonov et al. (2003) and Gardner et al. (2006) closely match the relationship between POC and K_{490} at mid to high concentrations, but deviate more at lower concentrations (Fig. 3b).

3.3. Spectral Radiance and Surface POC Concentration

Our second approach employs empirical regressions to quantify correlations between the spectral radiance and surface POC concentration. The depth of penetration within the water column is wavelength-dependent. Gordon and McCluney (1975) showed that 90% of all remotely-sensed ocean color radiance originates from the upper layer - the first optical depth (z_{90}), which is the depth at which radiance decreases to 1/*e* of the incident radiance values (=1/K_{490}). Normally it has been assumed that radiance can be linearly integrated down and up through the water column, however, Zaneveld et al. (2005) show that although this is true if all radiance comes from an optically well-mixed layer (i.e. homogeneous), the integration should be exponential over non-homogeneous optical depths.

SeaWiFS measurements of the spectral radiance upwelled from the ocean during NEGOM cruises were acquired at every POC station using 6 wavelengths over the full SeaWiFS spectral range of 412-670 nm (Fig. 4a). However, the 58-point synchronously matched data set was not large enough to delineate the radiance curves for different POC concentration ranges. Therefore we combined all binned radiance and POC data during each cruise day to test how the radiance varied as a function of POC concentration. The radiance means were between 0.05 and 1.37 (mw/cm^2/μm/sr), and the standard error at each wavelength ranged from 0.00005 to 0.0612 (0.005 to 6.12 %).

POC concentration *versus* radiance shows a relationship that changes as a function of POC concentration (Fig. 4a). Not surprisingly, this is very similar to the relationship demonstrated and modeled between R_{rs} *versus* wavelength at varying chlorophyll *a* concentrations (e.g. Morel & Maritorena, 2001; Werdell & Bailey, 2005).

When the POC concentration in the surface water increases, the peak in radiance shifts from the shorter wavelengths (412 and 443 nm, violet-blue band) to longer wavelengths (to 490 nm and then 555 nm, green band). As with chlorophyll, radiance at 510 nm remains relatively constant over a wide range of POC concentrations (20 <POC <550 mg/m^3). In particle-free water, the depth of light penetration decreases by a factor of about 20 from blue to red wavelengths. Thus, radiance at shorter wavelengths comes from a much thicker water column than at long wavelengths, and water reflectance dominates the signal. The depth of light penetration also diminishes as the concentration of POC, chlorophyll, inorganic particles, etc. increases. When POC concentration increases, the radiance peak shifts toward longer wavelengths because reflectance from particles in the water dominates over water reflectance (Fig. 4a and 4b).

3.4. Empirical Approaches between POC and Spectral Radiance (or Reflectance)

Re-plotting the data from Fig. 4a to show POC concentration as a function of L_{wn} reveals non-linearity at shorter wavelengths (412 - 510 nm; Fig. 4b). The relationship is more linear at 555 nm, but still produces considerable scatter (R^2=0.70, N=58; Table 1). The relationship is most linear at 670 nm, but the radiance range is small. Thus, it is difficult to predict POC concentration based on radiance using a single wavelength. Therefore it is not surprising that correlations between POC and chlorophyll or K_{490} are much better than a single wavelength radiance because chlorophyll and K_{490} are both based on a ratio of radiances at two wavelengths.

Using a multiple-wavelength approach, one is more likely to distinguish multiple or shifting radiance peaks resulting from multiple or compound particle types in the water column, thus improving the correlation with POC. To improve upon the limitations of a single-wavelength correlation, and to be independent of chlorophyll and K_{490} determinations, we adapted a multiple wavelength approach originally developed for land vegetation, known as the Normalized Difference Vegetation Index (NDVI) (Deering et al., 1975; Rouse et al., 1974). We refer to it here as the Normalized Difference Carbon Index (NDCI). Fig. 4a reveals that when surface POC concentration increases, the radiance peak shifts toward longer wavelengths. Thus, in our third approach the NDCI algorithm uses the difference of radiance between one blue and one green wavelength divided by their sum to estimate the concentration of POC:

$$POC = 10^{(1.08\times NDCI\_Lwn^3 + 1.09\times NDCI\_Lwn^2 + 1.37\times NDCI\_Lwn + 2.26)}, \text{ or}$$

$$POC = 10^{(1.08\times NDCI\_Rrs^3 + 1.06\times NDCI\_Rrs^2 + 1.34\times NDCI\_Rrs + 2.24)} \quad (4)$$

where $NDCI\_Lwn = \left[\frac{(L_{wn}(555) - L_{wn}(443))}{(L_{wn}(555) + L_{wn}(443))}\right]$, or $NDCI\_Rrs\left[\frac{(R_{rs}(555) - R_{rs}(443))}{(R_{rs}(555) + R_{rs}(443))}\right]$.

NDCI values are directly (but not linearly) proportional to POC concentrations (R^2=0.97, N=58, Fig. 5a and 5b), and are best fit with a cubic polynomial. The 443 nm radiance maximum in the NDCI corresponded best with POC concentrations less than 200 mg/m^3 and the 555 nm radiance maximum with POC concentrations greater than 200 mg/m^3 (Fig. 5b). At low (<200 mg/m^3) POC values (which were best related to the 443 nm radiance maximum) samples included both high and low %POC (Fig. 5a and 5b), while high POC values (>300 mg/m^3), (which were best related to the 555 nm radiance

maximum) were all samples with low %POC (Fig. 5a and 5b). Using two radiance maxima (443 and 555 nm) tended to decrease the noise level regardless of the concentration or percentage of inorganic and organic constituents.

Our fourth approach builds on the NDCI and is referred to as the Maximum Normalized Difference Carbon Index (MNDCI). It uses the approach developed in the SeaWiFS chlorophyll *a* algorithm OC4v4 (O'Reilly et al., 2000) of selecting the maximum radiance band of all blue-to-green wavelengths, though we use 412, 443 and 490 rather than 443, 490 and 510 as used in OC4v4. As noted in O'Reilly et al. (1998), this has the potential advantage of maintaining the highest possible satellite sensor signal:noise ratio over a broad range of POC concentrations. They note that multiple band ratios may also be useful in operationally differentiating different ocean realms with respect to trophic status, based on the concentration boundaries over which each band dominates. In the green wavelengths, peaks (which occurred at concentrations >~160 mg/m^3), were consistently at 555 nm, so radiance at 555 nm was used as the long wavelength reference. Normalized ratios should be less sensitive to errors in the atmospheric correction than the simple magnitude of normalized water leaving radiance at a single wavelength, yielding:

$$POC = 10^{(4.36\times MNDCI\_Lwn^5 + 1.77\times MNDCI\_Lwn^4 - 1.98\times MNDCI\_Lwn^3 - 0.21\times MNDCI\_Lwn^2 + 1.78\times MNDCI\_Lwn + 2.45)} \text{ , or}$$

$$POC = 10^{(6.36\times MNDCI\_Rrs^5 + 3.26\times MNDCI\_Rrs^4 - 0.37\times MNDCI\_Rrs^3 - 0.40\times MNDCI\_Rrs^2 + 1.79\times MNDCI\_Rrs + 2.42)} \quad (5)$$

where $MNDCI\_Lwn = \left[\frac{\{L_{wn}(555) - \max(L_{wn}(412), L_{wn}(443), L_{wn}(490))\}}{\{L_{wn}(555) + \max(L_{wn}(412), L_{wn}(443), L_{wn}(490))\}}\right]$ or

$$MNDCI\_Rrs = \left[\frac{\{R_{rs}(555) - \max(R_{rs}(412), R_{rs}(443), R_{rs}(490))\}}{\{R_{rs}(555) + \max(R_{rs}(412), R_{rs}(443), R_{rs}(490))\}} \right].$$

MNDCI values are directly (but not linearly) proportional to POC concentrations and are fit with a fifth-order polynomial (Fig. 5c and 5d). Although a cubic polynomial produced an excellent fit to the data (R^2=0.99), the fifth-order polynomial fit the data better at low concentrations (<30 mg/m^3), yielding lower values than a cubic fit. Because a large portion of the open ocean is in this low-concentration range it is important to obtain accurate estimates in that concentration range. The MNDCI algorithm produces better results than the first three approaches, especially when predicting high POC concentrations (R^2=0.99, N=58).

Evaluation of the dominant radiance in the MNDCI as a function of POC concentration demonstrates that the 412 and 443 radiances best predict POC concentration when POC <60 mg/m^3, the 490 radiance when 60 <POC < 300 mg/m^3, and the 555 radiance when POC >300 mg/m^3 (Fig. 5d). POC concentrations >300 mg/m^3, which were best predicted by the long wavelength radiance (555 nm) were dominated by samples with <25% POC (Fig. 5c and 5d). This multispectral approach using NDCI or MNDCI makes the POC estimates more accurate than using single wavelength or radiance ratio algorithms, especially in waters containing a mixture of organic (living and non-living) and inorganic particulate components.

Plotting NDCI versus MNDCI values (Fig. 6) shows close agreement between the two algorithms when both values were less than -0.4 (<~65 mg/m^3) because both algorithms use similar band ratios over most of that range (Fig. 5b and 5d). The root

mean square error (RMSE) for both NDCI and MNDCI was similar (5.9 and 4.1 mg/m^3) whether POC % was > 25 or <25. Low POC concentration areas are generally located offshore and the blue bands have the highest peaks of the six wavelengths.

The difference in predicted POC between the two algorithms increased as the index exceeded -0.2 because the MNDCI used the maximum of three wavelengths (412, 443, 490 nm) rather than a fixed wavelength (443 nm) for NDCI. In the 100~200 mg/m^3 range (Fig. 6), the RMS errors of NDCI and MNDCI were about 30 and 14 mg/m^3 respectively for POC percentages > and < 25%. While the NDCI errors were similar for POC >25% and <25% (30 and 31 mg/m^3), the difference between POC >25% and <25% was larger using MNDCI (9 and 18 mg/m^3 respectively), but the MNDCI errors were much smaller in both %POC ranges. Where POC concentrations were 200 and 300 mg/m^3, total PM concentration varied from 500 to 1,600 mg/m^3. For samples where POC concentration >300 mg/m^3, total PM concentration ranged from 1,800 to 15,000 mg/m^3. The RMS errors of MNDCI were smaller than for NDCI (~ 33 versus 90 mg/m^3 where POC concentration >200 mg/m^3). Samples with higher POC and PM concentrations were geographically constrained between the Mississippi River and Mobile Bay, an area highly influenced by input of inorganic particle.

Although Ahn et al. (2006) identified different spectral responses of various water constituents in remotely sensed radiance (or reflectance), we cannot independently separate or extract the signal created by each component. Retrieval of compositional data becomes even more difficult in waters where the signal from a small quantity of POC is masked by the signal from a large quantity of inorganic particles or CDOM, which

constitutes ‘noise’ for our purposes. It is not always easy to optically differentiate CDOM from detrital material, as the two have similar absorption spectra (Carder et al., 1999; Garver & Siegel, 1997; Maritorena et al., 2002; Roesler & Perry, 1995), although Hu et al. (2003) found very good correlations between CDOM and SeaWiFS data during the NEGOM cruises, Siegel et al. (2002) have developed algorithms for CDOM in the open ocean, and Gould et al. (2002) and Stavn and Richter (2008) have partitioned the contributions to optical properties from particulate organic and inorganic components in the Gulf of Mexico.

3.5. POC Estimates in low %POC Waters

Fig. 7 and Table 1 provide correlation plots and statistical data between discrete POC measurements and POC estimates obtained using four different algorithms (equations 2-5) using samples where POC >25%, <25%, and combined. To provide a quantitative algorithm evaluation, the mean ratio values between the *in situ* POC and POC estimates, as well as the corresponding standard deviation are calculated (Table 1). While these tests validate the fits of our data, it is not an independent verification of the algorithms. The root mean square errors (RMSE), mean ratio, and standard deviation for all algorithms were smaller for POC samples where POC >25% than for POC samples where POC <25%.

The Normalized Difference Carbon Index (Fig. 5a, 5b, and Eq. 4) using two bands ($L_{wn}(443)$ and $L_{wn}(555)$) greatly reduces scatter between predicted and sampled data compared to the single-wavelength algorithm ($L_{wn}(555)$, Table 1). While NDCI

values are well correlated with POC whether POC is >25% or <25% (Fig. 7c and Table 1), the Maximum Normalized Difference Carbon Index algorithm produced a slightly better correlation between *in situ* POC and derived POC values at all concentrations (Fig. 5c, 5d, and Eq. 5). Furthermore, the slope, R^2, RMSE, mean ratio, and standard deviation are more uniform for the MNDCI whether the %POC range was >25%, <25%, or all samples combined (Fig. 7d and Table 1).

The potential errors of POC algorithms in low %POC waters could become unreasonably large because the presence of terrigenous sediments and CDOM creates an optically complex environment. Either we can develop different algorithms for high %POC and low %POC waters and have some means of classifying which type of water is being sampled, or we can develop more complex algorithms that can be applied in either high %POC or low %POC waters, and in waters transitional between the two. The results in Figs. 5, 6 and 7 suggest that obtaining the best POC estimates in complex waters requires complex algorithms using at least 2 wavelengths, and ideally 4 wavelengths rather than a single wavelength, chlorophyll, or K_{490} as previously used for high %POC waters. The use of chlorophyll or K_{490} in an algorithm involves the use of the 2 wavelengths used to derive either of those parameters, thus using more than one wavelength. The wavelength ratios proposed by Stramski et al. (2008) also meet this criterion.

Here we attempted to use data about the POC percentage of PM in samples to differentiate between high %POC and low %POC waters. However, one does not always have the luxury to measure total PM because of the volume of water required. One

important result from this study is that the POC estimates by both the NDCI and MNDCI algorithm give nearly the same %POC estimate regardless of whether POC in the samples is >25% or <25%, suggesting that both algorithms could be used in either high %POC or low %POC waters (Fig. 7 and Table 1).

3.6. Seasonal Pattern of POC

The original purpose of the NEGOM study was to investigate the spatial and temporal distribution of hydrographic variables to understand physical processes on the continental shelf and slope of the northern Gulf of Mexico. Although the NEGOM study significantly expanded our understanding of the distribution of POC based solely on bottle data, any study restricted to discrete shipboard water samples (especially in dynamic coastal waters) is highly limited because of the time and labor required for sampling. We need remote sensing approaches to assess the temporal and spatial variability of POC at much higher resolution to adequately understand and monitor complex marine environments. Thus, we used the available NEGOM data to develop the most accurate algorithms possible to assist us in this endeavor. We note here some of the major spatial/temporal observations and how the improved resolution from the MNDCI algorithm clarified POC distributions in the study area (compare Fig. 8 and 9).

Maps of POC distribution in the Gulf of Mexico (Fig. 9) were created using the MNDCI algorithm and ocean color data collected by SeaWiFS. Note that the resolution of the maps in Fig. 9 is about 1.1 km, whereas the maps in Fig. 8 were contoured from ~ 60 data points shown on each map, with station spacing from 10-100 km. In the MNDCI

POC algorithm, some data points which yield negative water-leaving radiance at shorter wavelengths and were removed from each map in Fig. 8. The close comparison with measured POC (Fig. 8) and the 0.99 correlation coefficient in Fig. 5c and 5d are strong evidence that spectral variations are more closely tied with POC concentration than other optical properties of sea water (Fig. 8 and 9). However, high resolution POC maps (Fig. 9) show much more detailed spatial patterns of POC than are discernable in Fig. 8.

The most notable difference between Figs. 8 and 9 is that with satellite coverage we are able to fill in both seaward and coastal areas which were excluded during shipboard sampling. Some of those coastal areas had high POC concentrations, but they were within the range of POC concentrations directly sampled around the Mississippi Delta region. One caveat about the estimates west of Florida is that Florida is a carbonate platform and the few rivers in that region are likely to carry much less siliciclastic sediment than is found west of the Florida panhandle. Filling in the seaward areas of the sampling region is highly justified given the large number of samples from regions with similar low concentrations.

A second notable difference is the much greater spatial constraint of the boundaries of features (e.g. N3, N6 and N9; Fig. 8 and 9). During those summer cruises the loop current and eddies draw water from the Mississippi area out beyond the shelf into the open Gulf waters. These features are far more patchy than can be determined with coarse bottle sampling. It is obvious that even if bottle samples had been obtained in coastal areas, the patchiness exhibited along the Florida coast and around the Mississippi Delta using satellite data (e.g. N2 in Fig. 9) would not have been revealed.

A comparison of the range of POC concentrations between bottle and algorithm estimates for identical areas shows that the NEGOM bottle POC concentrations ranged from 15 to 771 mg/m^3, while the range of MNDCI POC concentrations within the area circumscribed by the bottle stations was 13 to 984 mg/m^3 (area in Fig. 8). Higher POC concentrations were generally observed during the summer (May-August cruises) and lower values occurred during the fall (November cruises; Fig. 8 and 9). This is even more apparent in Fig. 9 by excluding the coastal values made possible with satellite data. The geometric mean based on 60 POC bottle stations per cruise was 139 ± 51 mg/m^3 for all summer seasons and 64 ± 17 mg/m^3 for all fall seasons. After mapping the area using MNDCI-based POC, the geometric mean for all pixels within the area circumscribed by the bottle stations was 150 ± 56 mg/m^3 for the summer seasons and 90 ± 43 mg/m^3 for the fall seasons, suggesting that the bottle estimates were low for the fall seasons probably due to artifacts of sampling coverage.

The 1998 summer mean for bottle POC values (167 mg/m^3) was far greater than the mean for all 9 cruises (100 ± 44 mg/m^3). Likewise, the 1998 summer MNDCI mean (175 mg/m^3) was greater than the MNDCI mean for all 9 cruises (113 ± 42 mg/m^3). The variations of surface POC concentrations roughly corresponded with those of surface particulate matter (PM) and varied seasonally in a similar fashion, although the variations were slightly greater for bottle PM than for bottle POC (Son, 2006).

During all seasons, surface POC concentrations of over 100 mg/m^3 occurred over the inner shelf across the entire region. Concentrations significantly greater than 100 mg/m^3 were confined to the inner shelf along the midsection and eastern portion of the

study area but extended over the narrow outer shelf near the Mississippi delta. Over the rest of the outer shelf and the upper slope, concentrations dropped off rapidly, to <100 mg/m^3 at the seaward of the study area (Figs. 8 and 9). Fresh-water input from all major rivers, which lowered surface salinity (<33), was greater during 1997 and 1998 than during 1999 and 2000 and was associated with higher surface POC concentrations during 1997 and 1998 (Son, 2006), presumably resulting from increased nutrients and primary production.

Interannual variability in the spatial distribution of POC was much smaller in the fall and spring cruises than during summer cruises (Fig. 8 and 9). During the summer, a patchy swath of elevated surface POC waters (>300 mg/m^3) stretched from the shelf east of the Mississippi River over the upper slope in a northwest-southeast direction (Fig. 8 and 9). River inputs from the Mississippi and Alabama regions during the summer of 1998 were higher compared to 1999 and 2000 (N6 and N9) (Son, 2006). Lower surface-salinity waters extended out of the upper slope in the midsection of the study area and this spatial pattern was inversely correlated with surface temperature (Son, 2006). Hu et al. (2003) noted that during the summers of 1998 and 1999, a warm-core eddy was centered east of the Mississippi River delta that entrained low salinity, high chlorophyll and high CDOM surface waters. These waters were also high in POC.

4. Conclusions

Estimates of upper ocean parameters using remote sensing data are increasingly made by developing empirical algorithms because shipboard sampling will always be inadequate for studying dynamic surface processes due to limited resolution on both spatial and temporal scales. Using a large 3-year, seasonal data set that included *in situ* measurements and satellite-derived ocean color products, we tested several simple empirical approaches to derive POC concentrations based on data from SeaWiFS's chlorophyll, K_{490}, and radiance measured at six wavelengths in the visible spectral range using least-squares fit regressions. Two SeaWiFS products (chlorophyll concentration and K_{490}) were reasonably well correlated with temporal and spatial variations of surface POC concentrations.

Our analysis of the spectral response demonstrated that the radiance was significantly dependent on POC concentration, and that the radiance peak shifted significantly from violet-blue wavelengths to green wavelengths as POC concentration increased. Based on this spectral dependence, it was demonstrated that using multiple wavelength radiances was more sensitive to complex marine environments than those using single wavelength radiance or blue-to-green ratios, and provided more reliable estimates over a wide range of surface POC concentrations. This also suggests that a multispectral approach might improve correlations between in situ c_p and POC.

In this study, the best estimates for POC concentrations were achieved with the Maximum Difference Carbon Index algorithm (R^2=0.99). It is significant that the accuracy of the multi-spectral MNDCI algorithm was not significantly different whether

used in high or low %POC waters. Not having to determine whether waters of interest are high %POC versus low %POC waters is an important advance. This approach is promising for mapping POC concentrations regionally based on remote sensing data because such algorithms clearly reproduce the seasonal cycles and spatial distribution in the Gulf of Mexico at much greater resolution than is possible using just bottle samples or POC-calibrated optical profiles of c_p at ship stations. This is particularly important for interpreting POC cycling in dynamic waters such as those in the Gulf of Mexico. While these algorithms are regionally tuned, our analysis approach should be useful for developing algorithms elsewhere for estimating and monitoring changes in POC concentrations at regional, to perhaps global scales, including low %POC shelf waters.

ACKNOWLEDGMENTS

We thank Christina Bernal for collecting the shipboard data for this paper as part of her TAMU thesis work during the Minerals Management Service's Northeastern Gulf of Mexico Physical Oceanography Program (NEGOM; OCS Study 98-0060). The help from scientists and technicians who participated in NEGOM is also appreciated. Support for YBS was provided by a Fellowship Texas A&M University. NSF grants OCE-9986762 and OCE-0137171 provided partial support. Discussions with Anthony Filippi and comments from reviewers were significantly helpful and appreciated. SeaWiFS data are the property of GeoEye Corporation, and their use here is in accordance with the SeaWiFS Research Data Use Terms and Conditions Agreement of the NASA SeaWiFS project and gratefully acknowledged.

REFERENCES

Afonin, E.I., Mishonov, A.V., & Yunev, O.A. (1992). Evaluation of the characteristics o f marine ultra-phytoplankton from remote waters colour sounding. *Oceanology*, *32* (6), 737-742.

Ahn, Y.H., Shanmugam, P., Ryu, J.H., & Jeong, J.C. (2006). Satellite detection of harmful algal bloom occurrences in Korean waters. *Harmful Algae*, 5, 213-231.

Bailey, S.W., McClain,C.R., Werdell, P.J., & Schieber, B.D. (2000). Normalized water-leaving radiance and chlorophyll *a* match-up analyses. *NASA Technical Memorandum*, *206892,* Greenbelt, MD.

Bailey, S.W., & Werdell, P.J. (2006). A multi-sensor approach for the on-orbit validation of ocean color satellite data products. *Remote Sensing of Environment, 102* ,12-23.

Baith, K., Lindsay, R., Fu, G., & McClain, C.R. (2001). Data analysis system developed for ocean color satellite sensors. *EOS*, *82*, 202.

Behrenfeld, M.J., Boss, E., Siegel, D., & Shea, D.M. (2005). Carbon-based ocean productivity and phytoplankton physiology from space. *Global Biogeochemical Cycles, 19*, GB1006 (doi:10.1029/2004GBoo2299).

Bernal, C.E. (2001). Spatial and Temporal Distributions of Particulate Matter and Particulate Organic Carbon, Northeast Gulf of Mexico, MS Thesis, Texas A&M University, College Station.

Bishop, J.K.B. (1999). Transmissometer measurement of POC. *Deep Sea Research I 46*(2), 353-369.

Bishop, J.K.B., Calvert, S.E., & Soon, M.Y.S. (1999). Spatial and temporal variability of POC in the northeast Subarctic Pacific. *Deep Sea Research II, 46,* 2699-2733.

Carder, K.L., Chen, F.R., Lee, Z.P., Hawes, S.K., & Kamykowski, D. (1999). Semianalytic moderate resolution imaging spectrometer algorithms for chlorophyll a and absorption with bio-optical domains on nitrate-depletion temperatures. *Journal of Geophysical Research, 104*(3), 5403-5421.

Cho, B.C., & Azam, F. (1990). Biogeochemical significance of bacterial biomass in the ocean's euphotic zone. *Marine Ecology Progress Series, 63*, 253-259.

Cho, K.W., Reid, R.O., & Nowlin, W.D. (1998). Objectively mapped stream function fields on the Texas-Louisiana shelf based on 32 months of moored current meter data. *Journal of Geophysical Research, 103*, 10377-10390.

Chung, S.P., Gardner, W.D., Landry, M.R., Richardson, M.J., & Walsh, I.D. (1998). Beam attenuation by microorganisms and detrital particles in the equatorial Pacific. *Journal of Geophysical Research, 103*, 12669-12681.

Deering, D.W., Rouse, J.W., Haas, R.H., & Schell, J.A. (1975). Measuring Forage Production of Grazing Units from Landsat MSS Data. *Proceedings, Tenth International Symposium on Remote Sensing of Environment, Ann Arbor: ERIM*, *2*, 1169-1178.

DiMarco, S.F., & Reid, R.O. (1998). Characterization of the principal tidal current constituents on the Texas-Louisiana shelf. *Journal of Geophysical Research, 103*, 3093-3109.

Dudek, A.V., Cunningham, A., & McKee, D. (2003). Regional validation of SeaDAS

algorithms and remote sensing of a complex frontal structure in the southern Irish Sea. *Proceeding Remote Sensing Ocean and Sea Ice 2003, 5233*, 69-76.

DuRand, M.D., Olson, R.J., & Chisholm, S.W. (2001). Phytoplankton population dynamics at the Bermuda Atlantic time-series station in the Sargasso Sea. *Deep Sea Research II, 48*, 1983-2003.

Eppley, R.W., Chavez, F.P., & Barber, R.T. (1992). Standing stocks of particulate carbon and nitrogen in the equatorial Pacific at 150°W. *Journal of Geophysical Research, 97*, 655-661.

Gardner, W.D., Walsh, I.D., & Richardson, M.J. (1993). Biophysical forcing of particle production and distribution during a spring bloom in the North Atlantic. *Deep Sea Research II, 40*, 171-195.

Gardner, W.D., Chung, S.P., Richardson, M.J., & Walsh, I.D. (1995). The oceanic mixed-layer pump. *Deep Sea Research II, 42*, 757-775.

Gardner, W.D., Richardson, M.J., Carlson, C.A., Hansell, D., & Mishonov, A.V. (2003). Determining true particulate organic carbon: bottle, pumps and methodologies. *Deep Sea Research II, 50*, 655-674.

Gardner, W.D., Mishonov, A.V., & Richardson, M.J. (2006). Global POC concentrations from in-situ and satellite data. *Deep Sea Research II, 53*, 718-740.

Garver, S.A., & Siegel, D.A. (1997). Inherent optical property inversion of ocean color spectra and its biogeochemical interpretation: 1. Time series from the Sargasso Sea. *Journal of Geophysical Research, 102*(C8), 18607-18625.

Gordon, H.R., & McCluney, W.R. (1975). Estimation of depth of sunlight penetration in

sea for remote-sensing. *Applied Optics, 14*, 413-416.

Gordon, H.R., & Wang, M. (1994). Retrieval of water-leaving radiance and aerosol optical thickness over the oceans with SeaWiFS: A preliminary algorithm. *Applied Optics, 33*, 443-452.

Gould, R.W., Jr., Stavn, R.H., Twardowski, M.S., & Lamela, G.M. (2002). Partitioning optical properties into organic and inorganic components from ocean color imagery. *Proceedings, Ocean Optics XVI, Santa Fe, New Mexico*.

Gundersen, K., Orcutt, K.M., Purdie, D.A., Michaels, A.F., & Knap, A.H. (2001). Particulate organic carbon mass distribution at the Bermuda Atlantic Time-series Study (BATS) site. *Deep Sea Research II, 48*, 1697-1718.

Hu, C., Muller-Karger, F.E., Biggs, D.C., Carder, K.L., Nababan, B., Dadeau, D., & Vanderbloemen, J. (2003), Comparison of ship and satellite bio-optical measurements on the continental margin of the NE Gulf of Mexico. *International Journal of Remote Sensing*, *24*(13), 2597–2612.

JGOFS (1996), Protocols for the Joint Global Ocean Flux Study (JGOFS) core measurements. Report #19, *Intergovernmental Oceanographic Commission*, 170pp., Bergen, Norway.

Lee, Z., & Hu, C. (2006). Global distribution of Case-1 waters: An analysis from SeaWiFS measurements. *Remote Sensing of Environment, 101*, 270-276.

Lohrenz, S.E., Dagg, M.J., & Whitledge, T.E. (1990). Enhanced primary production at the plume-oceanic interface of the Mississippi River. *Continental Shelf Research*, *10*, 639-664.

Loisel, H., & Morel, A. (1998). Light scattering and chlorophyll concentration in case 1 water: a reexamination. *Limnology and Oceanography, 43*, 847-858.

Loisel, H., Boss, E., Stramski, D., Oubelkheir, K., & Deschamps, P.-Y. (2001). Seasonal variability of the backscattering coefficient in the Mediterranean Sea based on Satellite SeaWiFS imagery. *Geophysical Research Letter, 28*, 4203-4206.

Maritorena, S., Siegel, D.A., & Peterson, A.R. (2002). Optimization of a semianalytical ocean color model for global-scale applications. *Applied Optics, 41*, 2705-2714.

McClain, C.R., Barnes, R.A., Eplee, J.R.E., Franz, B.A., Hsu, N.C., Patt, F.S., Pietras, C.M., Robinson, W.D., Schieber, B.D., Schmidt, G.M., Wang, M., Baily, S.W., & Werdell, P.J. (2000). SeaWiFS Postlaunch Calibration and Validation Analysis, *Part 2, SeaWiFS Postlaunch Tech. Rep. Ser.,* vol. 10, *NASA/TM-2000-206892*, edited by S. B. Hooker and E. R. Firestone, 57 pp, NASA, Greenbelt, MD.

McClain, C.R., Feldman, G.C., & Hooker, S.B. (2004). An overview of the SeaWiFS project and strategies for producing a climate research quality global ocean bio-optical time series. *Deep Sea Research II*, 51, 5-42.

Mishonov, A.V., Gardner, W.D., & Richardson, M.J. (2003). Remote sensing and surface POC concentration in the South Atlantic. *Deep Sea Research II, 50*, 2997-3015.

Mobley, C.D., Stramski, D., Bissett, W.P. & Boss, E. (2004). Optical modeling of ocean waters: Is the Case 1-Case 2 classification still useful? *Oceanography, 17*(2), 60-67.

Morel, A., & Maritorena, S. (2001). Bio-optical properties of oceanic waters: A reappraisal. *Journal of Geophysical Research, 106*, 7163-7180.

Morel, A., & Prieur, L. (1977). Analysis of variations in ocean color. *Limnology and*

Oceanography, 22(4), 709–722.

Morey, S.L., Martin, P.J., O'Brien, J.J., Wallcraft, A.A., & Zavala-Hidalgo, J. (2003). Export pathways for river discharged fresh water in the northern Gulf of Mexico. *Journal of Geophysical Research, 108*(C10), 3303 (doi:10.1029/20002JC001674).

Mueller, J.L. (2000). SeaWiFS algorithm for the diffuse attenuation coefficient, K(490), using water-leaving radiances at 490 and 555 nm. in *SeaWiFS Postlaunch Calibration and Validation Analysis, Part 3, SeaWiFS Postlaunch Tech. Rep. Ser.,* vol. 11, *NASA/TM-2000-206892*, edited by S. B. Hooker and E. R. Firestone, pp. 24-27, NASA, Greenbelt, MD.

Ohlmann, J.C., & Niiler, P.P. (2005). Circulation over the continental shelf in the northern Gulf of Mexico. *Progress in Oceanography, 64*, 45-81.

O'Reilly, J.E., Maritorena, S., Mitchell, G., Siegel, M.A., Carder, K.L., Garver, S.A., Kahru, M., & McClain, C.R. (1998). Ocean color chlorophyll algorithms for SeaWiFS. *Journal of Geophysical Research, 103*(11), 24937-24953.

O'Reilly, J. E., Maritorena, S., Siegel, D. A., O'Brien, M. C., Toole, D., Mitchell, B. G., Kahru, M., Chavez, F. P., Strutton, P., Cota, G. F., Hooker, S. B., McClain, C. R., Carder, K. L., Mu¨ ller-Karger, F., Harding, L., Magnuson, A., Phinney, D., Moore, G. F., Aiken, J., Arrigo, K. R., Letelier, R.,&Culver,M. (2000), Ocean Color chlorophyll *a* algorithms for SeaWiFS, OC2 and OC4: Version 4. in *SeaWiFS Postlaunch Calibration and Validation Analysis, Part 3, SeaWiFS Postlaunch Tech. Rep. Ser.,* vol. 11, *NASA/TM-2000-206892*, edited by S. B. Hooker and E. R. Firestone, pp. 9-27, NASA, Greenbelt, MD.

Rabalais, N.N., Turner, R.E., Justic, D., Dortch, Q., Wiseman, W.J., & Sen Gupta, B.K. (1996). Nutrient Changes in the Mississippi River and system responses on the adjacent continental shelf. *Estuaries, 19*, 386-407.

Redalje, D.G., Lohrenz, S.E., & Fahnenstiel, G.L. (1994). The relationship between primary production and the vertical export of particulate organic carbon matter in a river-impacted coastal system. *Estuaries, 17*, 829-838.

Roesler, C.S., & Perry, M.J. (1995). In situ phytoplankton absorption, fluorescence emission, and particulate backscattering spectra determined from reflectance. *Journal of Geophysical Research, 100*, 13279-13294.

Rouse, J.W., Hass, R.H., Schell, J.A., & Deering, D.W. (1974). Monitoring Vegetation Systems in the Great Plains with ERTS. *Proceedings, Third Earth Resources Technology Satellite-1 Symposium*, Greenbelt: NASA SP-351, 3010-317.

Sathyendranath, S., Prieur, L., & Morel, A. (1989). A three-component model of ocean colour and its application to remote sensing of phytoplankton pigments in coastal water. *International Journal of Remote Sensing, 10*(8), 1373-1394.

Siegel, D.A., Maritorena, S., Nelson, N.B., Hansell, D.A., & Lorenzi-Kayser, M. (2002). Global distribution and dynamics of colored dissolved and detritial organic material. *Journal of Geophysical Research*, *107,* 3228, doi:10.1029/2001JC000965.

Son, Y.B. (2006). POC algorithms based on spectral remote sensing data and its temporal and spatial variability in the Gulf of Mexico, Ph.D. thesis, 200 pp, Texas A&M Univ., College Station.

Stavn, R.H., & Richter, S.J. (2008). Biogeo-optics: particle optical properties and the

partitioning of the spectral scattering coefficient of ocean waters. *Applied Optics*, *47*(14), 2660-2679.

Stramska, M., & Stramski, D. (2005). Variability of particulate organic carbon concentration in the north polar Atlantic based on ocean color observation with Sea-viewing Wide Field-of-view Sensor (SeaWiFS). *Journal of Geophysical Research, 110*, C10018, doi:10.1029/2004JC002762.

Stramski, D., Reynolds, R.A., Kahru, M., & Mitchell, B.G. (1999). Estimation of particulate organic carbon in the ocean from satellite remote sensing. *Science, 285*, 239-242.

Stramski, D., Reynolds, R.A., Babin, M., Kaczmarek, S., Lewis, M.R., Röttgers, R., Sciandra, A., Stramska, M., Twardowski, M.S., & Claustre, H. (2008). Relationship between the surface concentration of particulate organic carbon and optical properties in the eastern South Pacific and eastern Atlantic Oceans. *Biogeosciences*, *5*, 171-201.

Vastano, A.C., Barron Jr., C.N., & Shaar, E.W. (1995). Satellite observations of the Texas current. *Continental Shelf Research*, *15*, 729-754.

Walker, N.D., Rouse, L.J., Rouge, B., Fargion, G.S., & Biggs, D.C. (1994). The great flood of summer 1993: Mississippi River discharge studied. *EOS*, *75*, 409.

Walker, N.D. (1996). Satellite assessment of Mississippi River plume variability: causes and predictability. *Remote Sensing of Environment*, *58*, 21-35.

Werdell, P.J., & Bailey, S.W. (2005). An improved in-situ bio optical data set of ocean color algorithm development and satellite data product validation. *Remote Sensing*

of Environment. *98*, 122-140.

Zaneveld, J.R., Barnard, A., & Boss, E. (2005). Theoretical derivation of the depth average of remotely sensed optical parameters. *Optical Express*, *13*, 9052-9061 (http://www.opticsinfobase.org/abstract.cfm?URI=oe-13-22-9052).

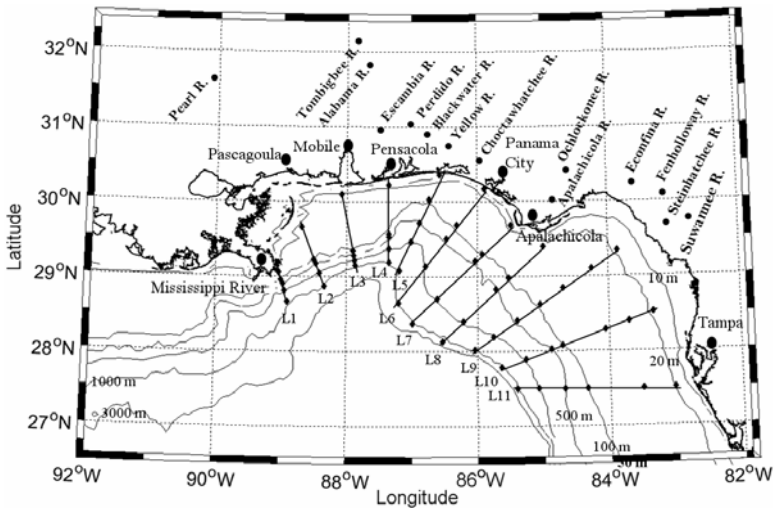

Fig. 1. Northeastern Gulf of Mexico (NEGOM) sampling grid occupied during 9 cruises from November 1997 to August 2000 (11 sampling tracks and 60 sampling stations).

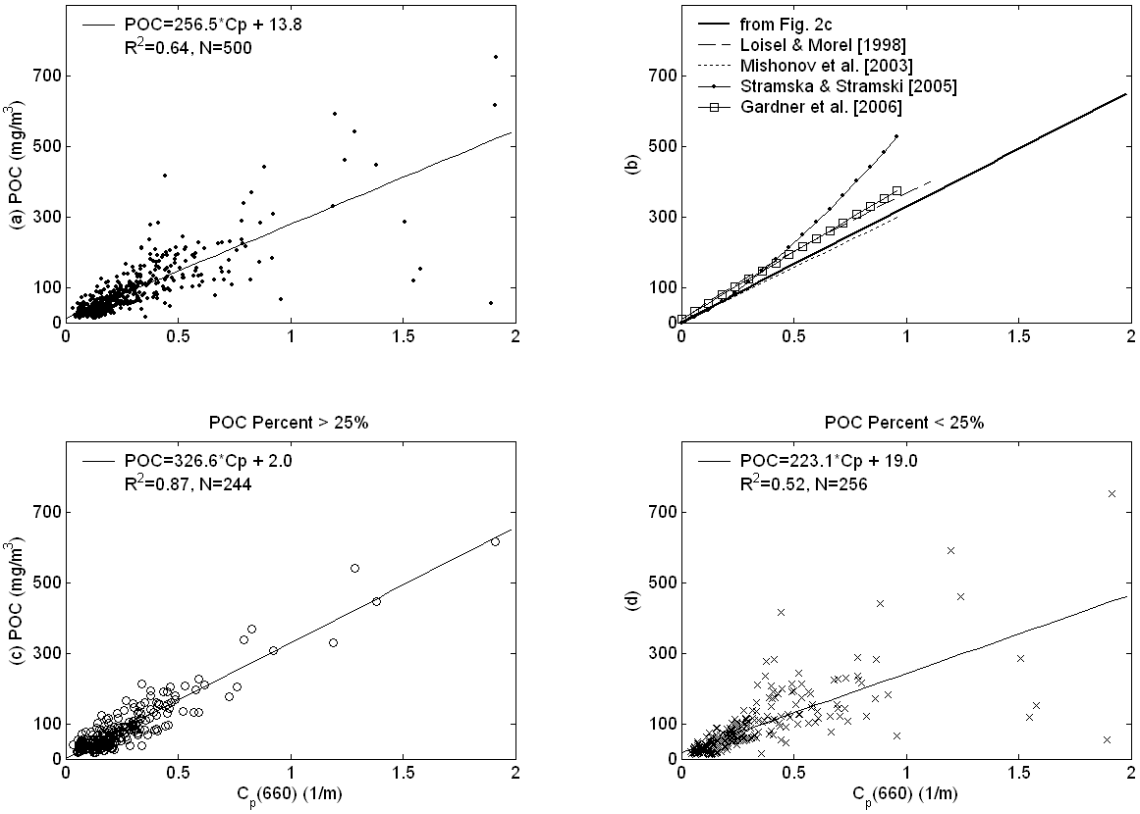

Fig. 2. (a) Surface POC concentration as a function of beam attenuation coefficient due to particles (c_p) during 9 NEGOM cruises. Scatter increased at high POC concentrations. (b) POC- c_p regressions from this and other studies. Separating samples by the percent of organic matter >25% (c) and <25% (d) revealed a very high correlation between POC and c_p with high percentages of organic matter and considerable scatter when inorganic particles were more abundant.

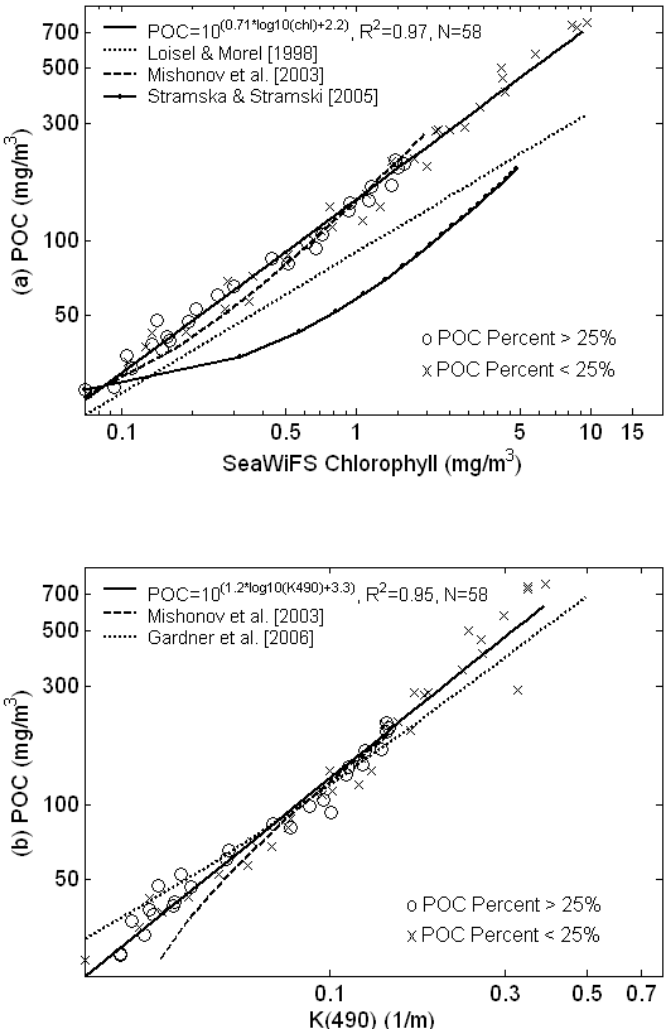

Fig. 3. A least-squares fit regression between NEGOM POC and (a) chlorophyll concentration and (b) diffuse attenuation coefficient at 490 nm. For comparison, our POC algorithm and four different algorithms from data in different areas are shown; Loisel and Morel (1998) - North Atlantic and Pacific open ocean; Mishonov et al. (2003) –South Atlantic open ocean; Stramska and Stramski (2005) –polar North Atlantic ocean, and Gardner et al. (2006) - Southern Pacific Ocean and Gulf of Mexico.

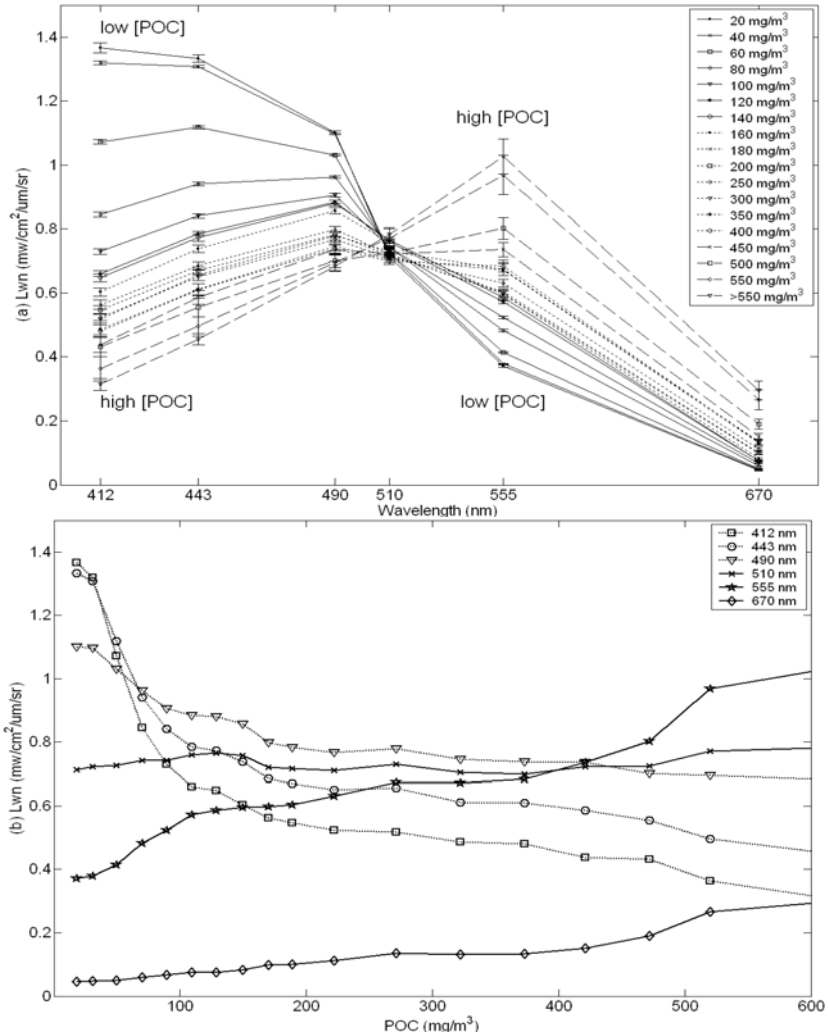

Fig. 4. (a) Normalized water-leaving radiance (L_{wn}) *versus* 6 SeaWiFS wavelengths averaged over areas with 18 different binned ranges of POC concentrations (1-750 mg/m^3) from all nine NEGOM cruises. Error bars are one standard deviation from the mean. The radiance peak shifts toward longer wavelengths as POC concentration increases. Radiance variation as a function of POC concentration is minimal at 510 nm. (b) L_{wn} *versus* averaged POC concentration from (a) at six spectral wave-bands.

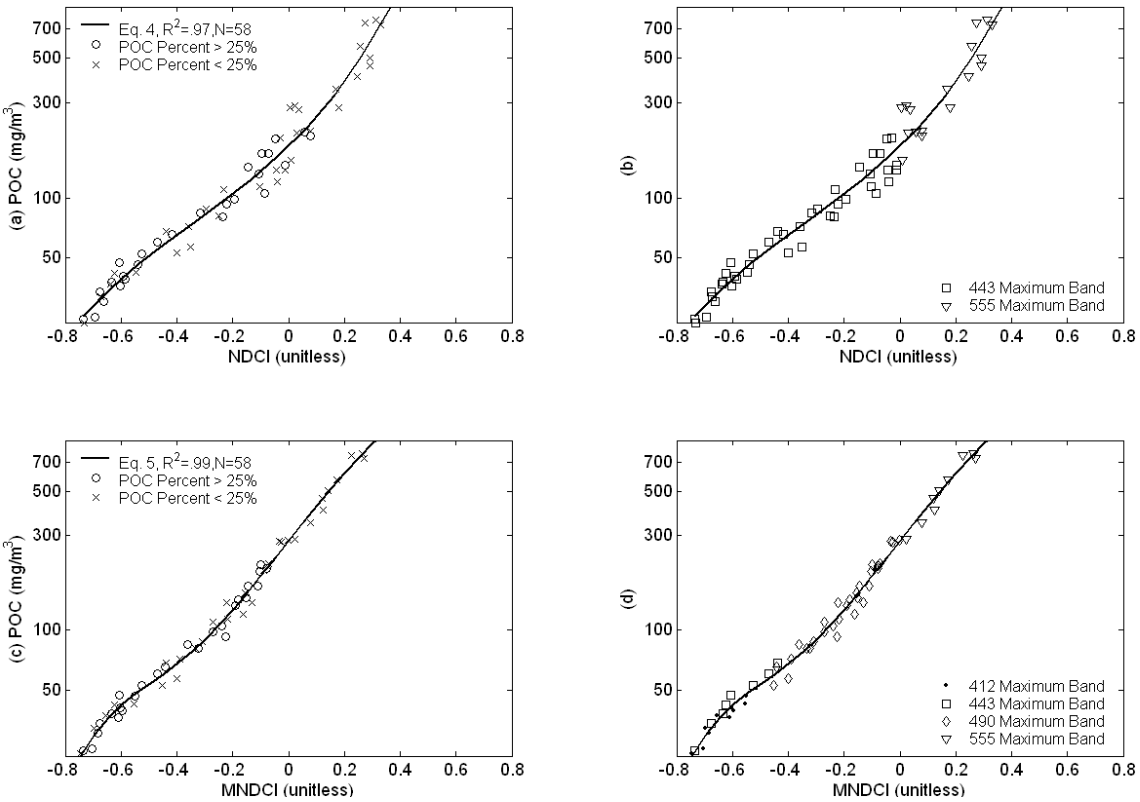

Fig. 5. Least-squares regressions between POC and (a, b) NDCI and between POC and (c, d) MNDCI. The NDCI uses two wavelengths, while the MNDCI uses the wavelength among 412, 443 and 490 nm with maximum radiance. Data points in (a) and (b) are the same, but are marked by the percent organic carbon in (a) and by the maximum wavelength band in (b). Data points in (c) and (d) are the same, but are marked by the percent organic carbon in (c) and by the maximum wavelength band ratio in (d). The MNDCI algorithm is more accurate at mid to higher POC concentrations than the NDCI algorithm.

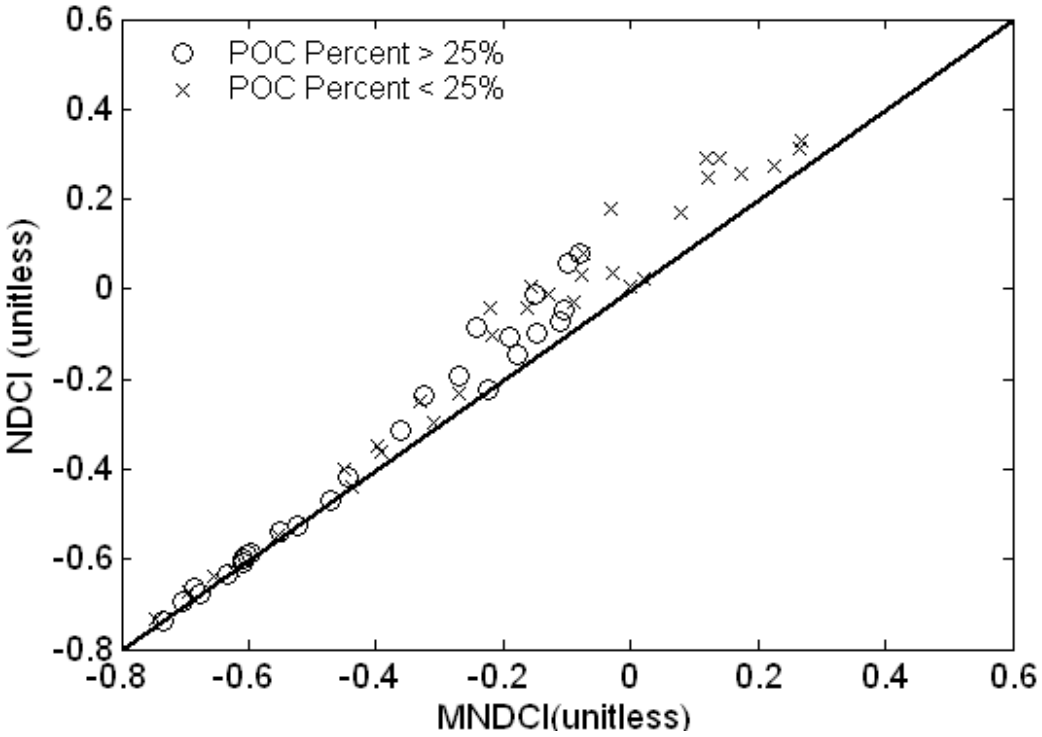

Fig. 6. Comparisons between NDCI and MNDCI POC algorithms.

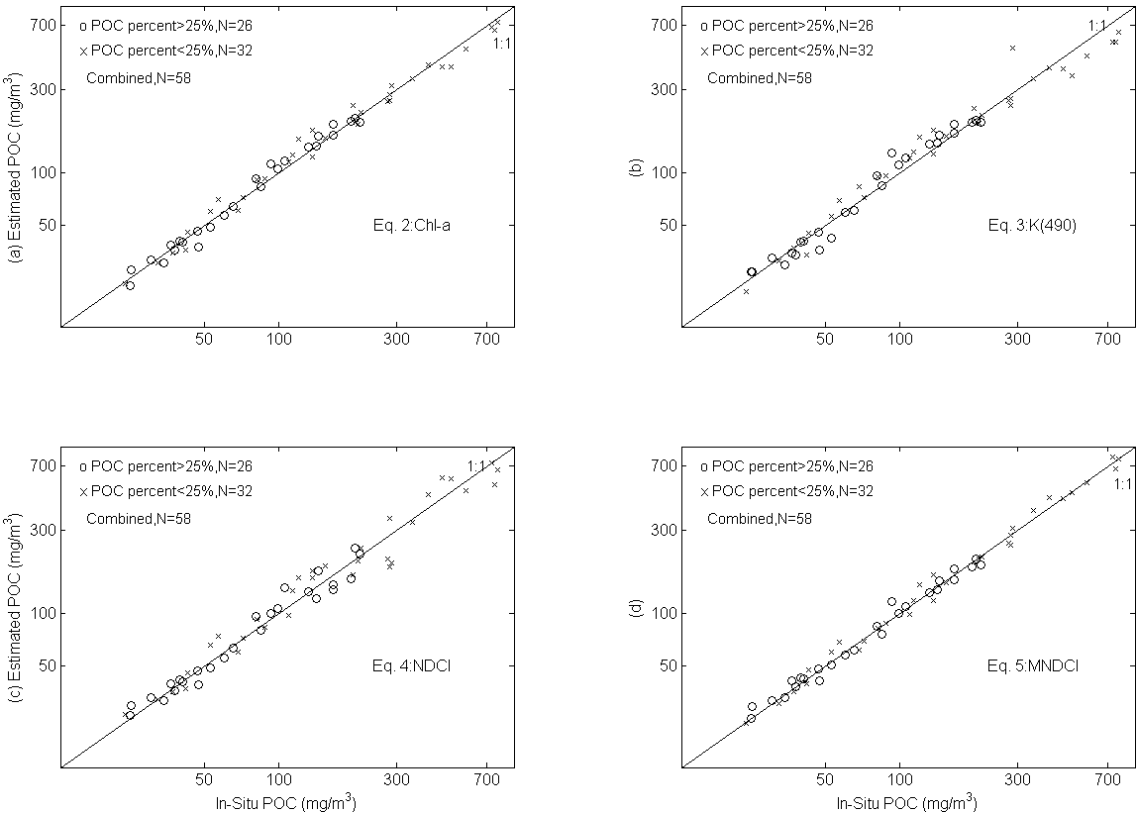

Fig. 7. Comparisons between *in situ* POC and estimated POC using four different algorithms based on SeaWiFS data and products. Data are delineated by percent particulate organic carbon >25% and <25%. All correlation statistics are in Table 1.

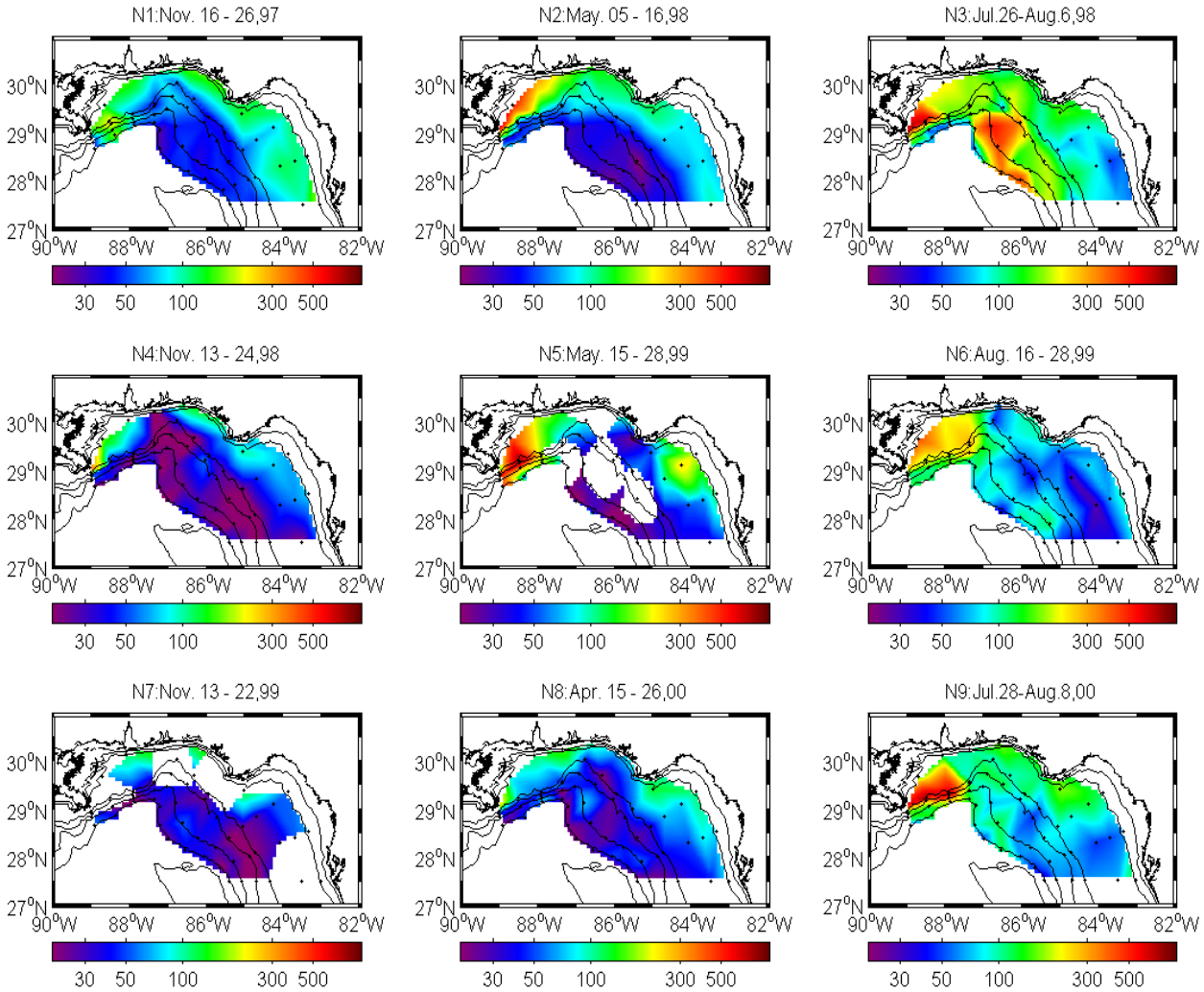

Fig. 8. Surface particulate organic matter concentration (mg/m^3) contoured from bottle samples collected at ~60 stations during each NEGOM hydrographic cruise. Cruises N1/N4/N7 were completed during fall, N2/N5/N8 - during spring, and N3/N6/N9 - during summer.

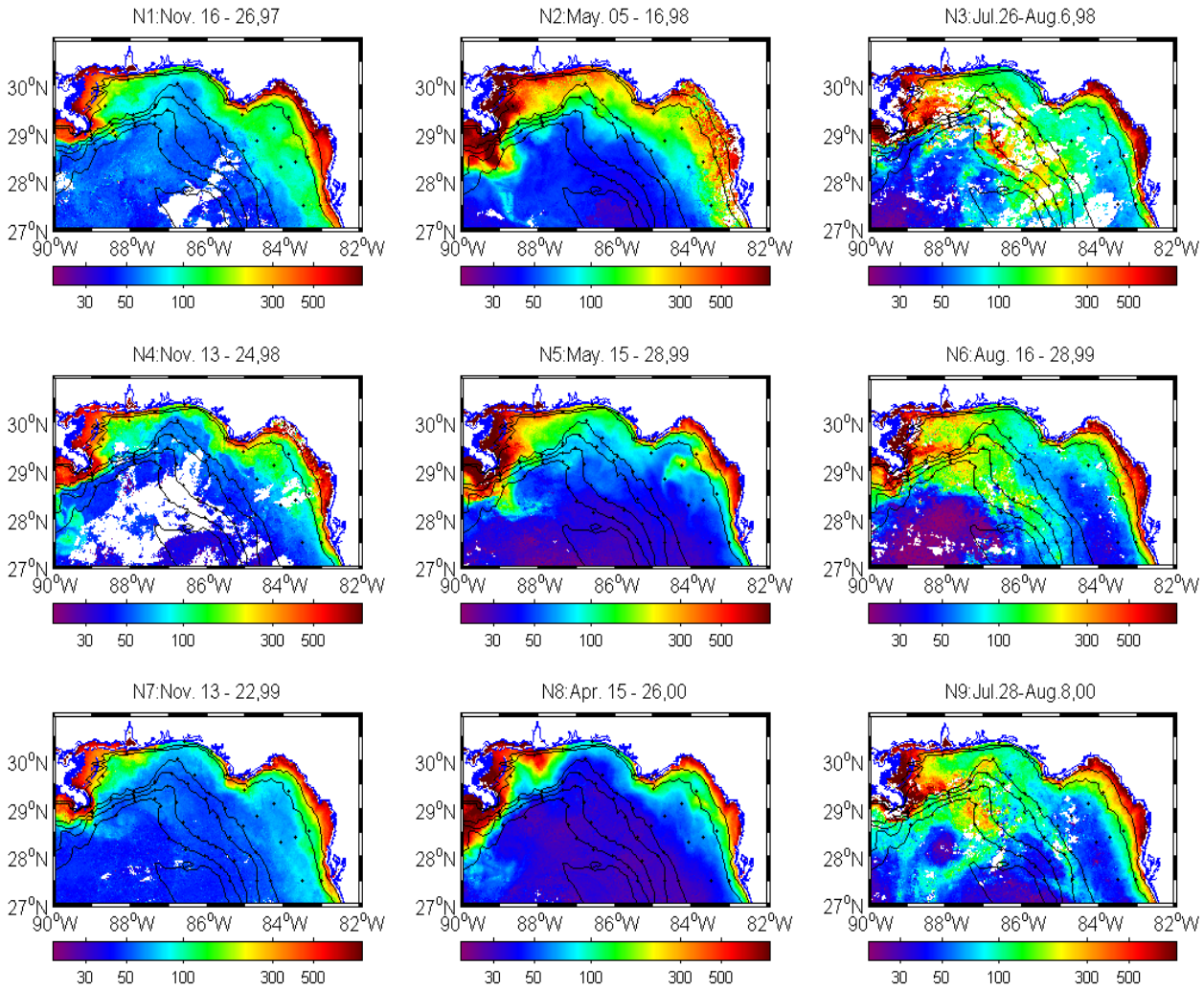

Fig. 9. Estimated POC concentration (mg/m^3) in the Northeastern Gulf of Mexico. Each map is compiled using the MNDCI (equation 5). POC estimates are well correlated with in situ data at both lower and higher POC concentrations (compare with Fig. 8, but note that maps in Fig. 8 used only ~60 points per image, whereas these images are based on a 1.1 km grid of data points).

Table 1. Regression (Type II) of in-situ POC versus estimated POC from algorithms: $RMSE = \sqrt{\frac{\sum(\log 10(estimate\_POC) - \log 10(in-situ\_POC))^2}{N-1}}$, mean ratio=$\frac{1}{N}\sum\left(\frac{\log 10(estimate\_POC)}{\log 10(in-situ\_POC)}\right)$, and the corresponding standard deviations are calculated with POC >25%, <25%, and combined POC samples.

	Percent POC	slope	intercept	R^2	RMSE	Mean Ratio	Standard Deviation	N
Lwn(555)*	>25% POC	0.521	0.908	0.635	0.184	1.020	0.099	26
	<25% POC	0.715	0.611	0.662	0.250	1.005	0.109	32
	combined	0.700	0.612	0.700	0.223	1.012	0.104	58
Eq. 2: Chl-a	>25% POC	1.035	-0.064	0.965	0.040	0.999	0.023	26
	<25% POC	0.966	0.072	0.966	0.051	1.000	0.025	32
	combined	0.987	0.026	0.967	0.046	1.000	0.024	58
Eq. 3: K(490)	>25% POC	1.045	-0.081	0.952	0.054	1.001	0.031	26
	<25% POC	0.936	0.139	0.944	0.082	1.001	0.037	32
	combined	0.969	0.064	0.950	0.071	1.001	0.034	58
Eq. 4: NDCI	>25% POC	0.978	0.040	0.964	0.056	1.000	0.029	26
	<25% POC	0.953	0.104	0.961	0.085	1.003	0.038	32
	combined	0.967	0.067	0.968	0.073	1.002	0.034	58
Eq. 5: MNDCI	>25% POC	0.972	0.052	0.986	0.035	1.001	0.020	26
	<25% POC	0.997	0.008	0.991	0.040	1.000	0.020	32
	combined	0.992	0.017	0.991	0.038	1.001	0.020	58

(* : Statistics for Lwn(555) not plotted in figures but are included here to emphasize the difference between single-wavelength and multiple wavelength approaches).